Energy Conversion and Management 115 (2016) 43–51

Contents lists available at ScienceDirect

Energy Conversion and Management

journal homepage: www.elsevier.com/locate/enconman

A mathematical model to investigate on the thermal performance of a flat plate solar air collector and its experimental verification

Chuan Sun [a,1], Yuting Liu [b,1], Chen Duan [c], Yao Zheng [a], Huawei Chang [a,*], Shuiming Shu [a]

[a] School of Energy and Power Engineering, Huazhong University of Science and Technology, Wuhan 430074, China
[b] China-EU Institute for Clean and Renewable Energy, Huazhong University of Science and Technology, Wuhan 430074, China
[c] Wuhan Second Ship Design and Research Institute, Wuhan 430064, China

ARTICLE INFO

Article history:
Received 16 November 2015
Accepted 15 February 2016

Keywords:
Flat plate solar air collector
Mathematical model
Mass flow rate
Thermal efficiency
Experimental verification

ABSTRACT

A mathematical model based on numerical finite-difference approach under forced convection mode was presented for the SAC. Airflow channel, absorber plate, glass cover, thermal insulation board and fan power were taken into consideration in this model and analyzed in detail. In order to verify the accuracy of this model, an indoor experimental system was built to study the performance of a double pass flow SAC. The effect of the inlet mass flow rate of the collector on the thermal performance was investigated under various environmental conditions. The outlet air temperature obtained from the theoretical and experimental studies are in reasonable agreement, which supports the validity of the theoretical model. By considering the energy gained and the fan power consumed under real conditions, the optimum mass flow rates were discussed and simulated with different ambient temperature and solar irradiance, which showed that for this flat plate SAC, $\dot{m}_{opt}$ equals 0.03 kg/s at I = 400 W/m^2, equals 0.04 kg/s at I = 700 W/m^2, and equals 0.045 kg/s at I = 1000 W/m^2. The results are useful for analyzing and designing new SACs.

1. Introduction

Solar collectors are devices that absorb the incoming solar radiation, convert it into heat and transfer the heat to the fluid flowing through them. According to the heat transfer medium flowing through the collector, solar collectors are divided into two types: Solar Liquid Collector (SLC) and Solar Air Collector (SAC). SACs are extensively used in air conditioning, agricultural product drying and industrial process heat [1,2]. Compared with SLCs, mass production of SACs appears to be inherently cheaper and easier to realize, since conductivity and corrosion of the absorber plate are secondary considerations [3]. However, the disadvantages of SACs are the low energy density, low thermal capacity and small heat conductivity of air. To improve the performance of SACs, qualitative or quantitative optimization suggestions to design efficient SACs are presented in many previous studies. These studies include different types of covers, selective surfaces, porous media, airflow channel geometries, fin structures, mass flow rate, inlet temperature, etc.

According to the types of flow channels, the conventional SACs can be constructed into three basic designs: SACs with air flow either over the absorber (type I) or under it (type II) and even on both sides of the absorber (type III). Close [3] compared the collection efficiencies of these three designs and found that the type with a stagnant air gap above the absorber plate might have the best performance. Duffie and Beckman [1] provided an example of an equation for flow over the absorber. In these two studies, the insulation of the back board was neglected which enhanced the impact of the heat losses through the cover. Parker et al. [4] improved Close's work by presenting procedures to compute thermal performance for the three types of collectors and compared the results with the experimental data. Thermal performance of SACs was also been predicted both theoretically and experimentally by Ong [5,6] and Njomo et al. [7].

Most studies focused on the enhancement of the thermal efficiency of SACs. For instance, Fudholi et al. [8] developed a theoretical model of a finned double-pass solar collector and carried out its experimental validation. Wei et al. [9] came up with a combined system of solar Kang and SAC to make the most of heat in cold winter and reduce air pollution. Stanciu [10] presented a theoretical study on the optimum tilt angle for flat plate collectors at different geographical locations and different time moments over a year. Also, tracking methods were analyzed and verified by Maia et al. [11], with which higher useful gain and higher efficiency could be reached. Baritto and Bracamonte [12,13] presented a dimensionless model for the outlet temperature of a non-isothermal

* Corresponding author. Tel.: +86 27 87542718.
E-mail address: changhuawei@hust.edu.cn (H. Chang).
[1] Chuan Sun and Yuting Liu contributed equally to the work.

http://dx.doi.org/10.1016/j.enconman.2016.02.048
0196-8904/

Nomenclature

k	thermal conductivity (W m^{-1} K^{-1})
c_p	heat capacity (J kg^{-2} K^{-1})
h	heat transfer coefficient (W m^{-2} K^{-1})
hr	radiative heat transfer coefficient (W m^{-2} K^{-1})
hc	convective heat transfer coefficient (W m^{-2} K^{-1})
T	temperature (K)
p	pressure (Pa)
u	velocity in x direction (m s^{-1})
v	velocity in y direction (m s^{-1})
$\dot{m}$	mass flow rate (kg s^{-1})
Pr	Prandtl number
I	solar radiation intensity (W m^{-2})
P	power (W)
K	K-factor
$\dot{V}$	volume flow rate
l	total length of the SAC
a	area (m^2)
w	thickness (m)
W	flow channel height
U	non-dimensionalized parameter of u
V	non-dimensionalized parameter of v
P	non-dimensionalized parameter of p
X	non-dimensionalized parameter of x
Y	non-dimensionalized parameter of y

Greek symbols

ν	kinetic viscosity (Pa s)
ρ	density (kg m^{-3})
α	absorptivity
τ	transmissivity
ε	emissivity
η	efficiency
σ	uncertainties/Stefan–Boltzmann constant
Θ	non-dimensionalized parameter of T

Subscripts

$f1$	airflow in channel I
$f2$	airflow in channel II
opt	optimum value
g	glass cover
$g-$	the lower surface of glass cover
$g+$	the upper surface of glass cover
b	insulation board
$b-$	the lower surface of insulation board
$b+$	the upper surface of insulation board
p	absorber plate
$p-$	the lower surface of absorber plate
$p+$	the upper surface of absorber plate
pg	value between absorber plate and glass cover
pb	value between absorber plate and insulation board
ga	value between glass cover and ambient
gp	value e between glass cover and absorber plate
ba	value between insulation board and ambient
bp	value between insulation board and absorber plate
in	inlet parameter
out	outlet parameter
a	ambient parameter
$theo$	theoretical value
exp	experimental value
fan	fan
$flow$	flow pump
f	flow friction
l	local resistance
u	useful thermal output value

SAC and it showed good agreement with experimental data. Another model was solved for a wide range of aspect ratios and mass flow numbers. Optimization studies on size, structure, fin geometry and flow control for flat plate SAC were also conducted by Badescu [14–16].

To balance the outlet temperature and thermal efficiency, exergy analysis could be considered in the evaluation of the airflow rate. A comparison of three types of SACs was conducted by Alta et al. [17] based on the energy and exergy analyses by which the optimized SAC designs were suggested. However, it is obvious that without any air leakage of the SAC, exergy efficiency always increases with the increasing of flow rate. Badescu proposed an optimal operation strategy for exergy gain maximization by controlling mass flow rate [18]. Farahat et al. [19] developed an exergetic optimization of flat plate solar collectors to determine the optimal performance and design parameters of these solar-to-thermal energy conversion systems. Jafarkazemi and Ahmadifard [20] carried out energetic and exergetic evaluation of SACs and found that increasing inlet water temperature and decreasing water mass flow rate can be effective on decreasing most of exergy destructions. Bahrehmand et al. [21] built a mathematical model for simulating the thermal behavior of single and two glass cover SAC systems with forced convection flow.

Another way to assess the performance of SAC is taking the fan power into consideration. El-Sebaii et al. [22] carried out a theoretical study on thermohydraulic efficiency of two types of SACs. One conventional way to enhance the thermal performance of SACs is to employ higher airflow rates but costs additional fan power and reduced the outlet temperature. An improved method is to lengthen the absorber and/or increase the depth of the channel. Hegazy [23,24] developed an analytical criterion for determining the optimal channel geometry in considering the fan power consumption.

Since most of the previous studies focused on the enhancement of the thermal efficiency of solar collectors with experimental study or numerical simulation, the theoretical analysis is usually conducted with only part of the components of the SACs. In their theoretical models, empirical equations or complex CFD (Computational Fluid Dynamics) simulation models are adopted. The work presented in this paper aims at providing a new, complete and fast mathematical model constructed in finite difference method to predict the thermal performance of a flat plate SAC and guide the design of flat plate SACs. The model is validated by comparing the simulation results with those obtained in an experimental model. It also aims at using the developed model to investigate the effects of the airflow rate on the comprehensive performance of a flat plate SAC and coming out with the optimum mass flow rates under different environmental conditions.

2. Theoretical study

2.1. Description of the presented SAC

The schematic of the SAC geometry is shown in Fig. 1. The SAC is covered by a single, high transmittance tempered glass with 3.2 mm thick, dimension size of 1944 × 932 mm. The heights of

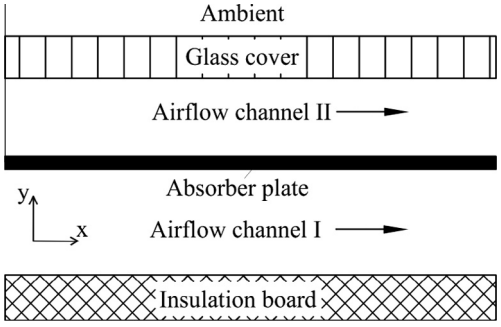

Fig. 1. Schematic of the solar collector model.

the airflow channel I and II are 25 mm and 15 mm, respectively. The absorber plate is a 0.4 mm-thick aluminum sheet with a selective coating on its irradiated surface. Mass flow rates in channel I and II are set to be 4/5 and 1/5 of the total mass flow rate, respectively.

The main heat transfer forms in the SAC are the radiation heat transfer from the solar radiation, the heat conduction of the glass cover and the absorber plate, as well as the convection heat transfer between the air flow and the glass cover plate and the absorbing plate. Solar energy penetrates the glass cover plate and shines on the absorber plate. The absorber plate absorbs heat from solar radiation and transfers heat convectively to the airflow above and below. Heat lost from the bottom of the collector to the environment is minimized by good thermal insulation, namely 20 mm phenolic foam board.

The flow and energy equations for the various elements of the SAC are formulated under the following simplifying assumptions: (i) Airflows in both of the two channels are assumed to be "parabolic flows", with developing velocity and temperature fields. (ii) Thermal inertias of the collector components are negligible because the total mass and the total thermal capacity of the SAC is low. (iii) Airflow is introduced into the SAC by suction at the outlet, so the initial velocity and temperature of the airflows are considered uniform, and the initial velocities are only in the x direction. (iv) Because the thickness of the SAC is much smaller than its width, very little heat and mass transfer happens in the z direction. Consequently, analyses are based on the two-dimensional model in Fig. 1. (v) No leakage occurs from the airflow channels. (vi) Thermal conductivity, kinematic viscosity and Pr of air are expressed as follows:

$$k\times 10^2 = 2.42758 + 0.00786T - 4.20342\times 10^{-6}T^2 + 1.08039\times 10^{-8}T^3 \tag{1}$$

$$v\times 10^6 = 13.27548 + 0.08694T + 1.39997\times 10^{-4}T^2 - 1.61033\times 10^{-7}T^3 \tag{2}$$

$$Pr = 0.70683 - 1.77369\times 10^{-4}T - 3.5554\times 10^{-7}T^2 + 3.12929\times 10^{-9}T^3 \tag{3}$$

Mathematical models based on numerical finite-difference approach for the flat plate double pass SAC under forced convection mode will be presented part by part. Fig. 2 shows the mesh of the discretized computational domain.

2.2. Airflow channel

At first, the flow patterns in the two channels are discussed. In all of the studied cases, the highest mass flow rate of the SAC is 0.05 kg/s. At such velocity, the Reynolds numbers of the airflows in the two channels are 2777 and 715. Taking that the inner surfaces are quite smooth and there is no blocking or interrupting in the two channels, the two airflows are considered laminar. And because the governing equations of the flow and heat transfer in developed domain is much simpler and just a special condition of those in developing flow, the airflow patterns in the channels of the SAC shown in Fig. 1 are considered to be steady-state, two-Dimensional, developing, and parabolic flowing. With the coordinate system shown in Fig. 1, the governing equations for the flows become [25]:

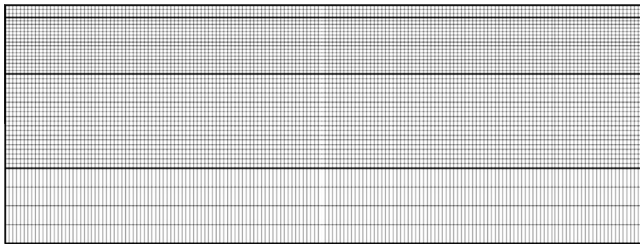

Fig. 2. Mesh of the discretized computational domain.

$$\frac{\partial v}{\partial y} + \frac{\partial u}{\partial x} = 0 \tag{4}$$

$$u\frac{\partial u}{\partial x} + v\frac{\partial u}{\partial y} = -\frac{1}{\rho}\frac{dp}{dx} + v\frac{\partial^2 u}{\partial y^2} \tag{5}$$

$$u\frac{\partial T}{\partial x} + v\frac{\partial T}{\partial y} = \frac{v}{Pr}\frac{\partial^2 T}{\partial y^2} \tag{6}$$

where u and v are the velocity of the flow in x direction and y direction, and p, T, ρ and v are the pressure, temperature, density and kinematic viscosity of airflow, Pr is the Prandtl number.

As shown in Fig. 2, the airflow channel I and II are divided into 1944 grids in the x direction, 20 grids and 16 grids in the y direction, respectively. After the equations being transformed into dimensionless form, the first-order upwind scheme and the second order central-difference scheme are used for discretization, which transforms the actual physical domain into the computational domain [26]. The discretization of Eqs. (4)–(6) are defined in the Appendix. A C++ program based on the model is prepared to get the velocity variation in the two airflow channels. The results are then substituted into the energy equation (A12) to solve the simultaneous heat transfer problem of the whole SAC.

2.3. Absorber plate

For the absorber plate of the SAC shown in Fig. 1, whose physical size in the y direction is so small and the thermal conductivity of the plate material is so large, we should obtain a reasonably uniform temperature distribution in the y direction. Consequently, the plate is divided into 1944 grids in x direction and only 1 layer in y direction.

After penetrating through the glass cover, solar irradiation is absorbed by the selective absorption film coated on the upper surface of the absorber plate, where it is transferred into thermal energy. Then, such thermal energy transfers into the airflows in the two channels through convection, conducts inside of the absorber plate, and exchanges between the absorber plate with the glass cover and the insulation board through thermal radiation. Accordingly, all nodal points are governed by the following energy equation:

$$\tau_g\alpha_p I = \sum_i hr_{pi}(T_p - T_i)dx_p + \sum_j k_{fj}(T_p - T_{fj})dx_p/dy_{fj} - 2k_p w_p \Gamma(p) \tag{7}$$

where hr is the radiative heat transfer coefficient, τ_g is the transmissivity of the glass cover, α_p is the absorptivity of the absorber plate, i represents glass and insulation board, j represents flow 1 and flow 2, k is the thermal conductivity, dx and dy are the differential increments in the x and y direction, and subscripts p, g, f_1 and f_2 indicate the absorber plate, the glass cover, the thermal insulation board, the airflow in channel I and II, respectively. $\Gamma(a)$ is the central difference scheme of parameter T_a, $\Gamma(p) = [(T_{p+} - T_p) - (T_p - T_{p-})]/2dx_p$, for example.

2.4. Glass cover and thermal insulation board

The glass cover and the thermal insulation board both have radiative and convective heat exchange with the ambient environment and radiative heat exchange with the absorber plate. In the x direction, the glass cover and thermal insulation board are divided into 1944 grids, and in the y direction they are divided into 3 grids and 4 grids.

For both of these two solid bodies, interior nodes are only governed by Fourier equation, while the governing equations of the exterior nodes on the upper and lower surfaces of the glass cover and of the thermal insulation board are defined as follows:

Glass cover:

$$hr_{ga}(T_g - T_a)dx_g + hc_{ga}(T_g - T_a)dx_g - k_g dy_g \Gamma(g) = 0 \tag{8}$$

$$hr_{gp}(T_g - T_p)dx_g + k_{f2}(T_g - T_{f2})dx_g/dy_{f2} - k_g dy_g \Gamma(g) = 0 \tag{9}$$

Thermal insulation board:

$$h_{rbp}(T_b - T_p)dx_b + k_{f1}(T_b - T_{f1})dx_b/dy_{f1} - k_b dy_b \Gamma(b) = 0 \tag{10}$$

$$hr_{ba}(T_b - T_a)dx_b + hc_{ba}(T_b - T_a)dx_b - k_b dy_b \Gamma(b) = 0 \tag{11}$$

$$hr_{pg} = \frac{\sigma(T_g + T_p)(T_g^2 + T_p^2)}{1/\varepsilon_g + 1/\varepsilon_p - 1} \tag{12}$$

$$hc_{ga} = 0.664k\ Pr^{1/3}\left(\frac{u_a}{\nu l}\right)^{1/2} \tag{13}$$

Where hr and hc represent the radiative and convective heat transfer coefficient, respectively. For example, hr_{pg} defined in Eq. (12) [25] represents the radiative heat transfer coefficient between the absorber plate and the glass cover; hc_{ga} defined in Eq. (13) [25] represents the convective heat transfer coefficient between the glass cover and the ambient. σ is the Stefan–Boltzmann constant, ε_g and ε_p are the emissivity of the glass cover and the absorber plate, u_a is the ambient wind velocity and l is the total length of the SAC. Other similar parameters can be defined in the same way.

The optical, radiative and conductive properties of the glass cover, the absorber plate and the thermal insulation board are listed in Table 1.

2.5. Grid independence examination

Grid independence study is conducted with total mass flow rate of air at 0.03 m^3/s, ambient and inlet temperature both at 21 °C, ambient wind velocity at 2 m/s and solar irradiance at 700 W. Two different grid sizes, 43 k and 86 k cells, are used. The temperature increase, iteration steps and calculation time of the two meshes are listed in Table 2. The differences in temperature increase between 86 k mesh and 43 k mesh is 1.1%. Therefore, the grid size of 86 k is selected.

Table 1
Optical and thermal properties of all components of the SAC.

τ_g	ε_g	k_g (W/mK)	α_p	ε_p	k_p (W/mK)	ε_b	k_b (W/mK)
0.91	0.84	0.8	0.95	0.1	221	0.9	0.027

Table 2
Grid independence examination.

Grid (k)	Temperature increase	Iteration steps (k)	Calculation time (s)
43	26.4	192	268
86	26.7	186	535

2.6. Fan power and comprehensive thermal performance

Electrical power is needed to drive the variable speed blower which forces the air throughout the SAC system. This amount of electrical energy depends on the fan efficiency and the flow pumping power. The flow pumping power could be estimated as:

$$P_{pump} = \dot{m}\Delta p/\rho \tag{14}$$

where Δp is the total pressure drop experienced by the airflow in passing through a certain channel due to flow friction and local resistance at channel entrance, exit and various joints:

$$\Delta p = \Delta p_f + \Delta p_l \tag{15}$$

Where Δp_f and Δp_l are the pressure drop caused by flow friction and local resistance, respectively. Δp_f in both of these two channels can be obtained from the numerical calculation of the airflow mentioned in Section 2.2. Δp_l is determined from the following equation:

$$\Delta p_l = \sum(K\rho u^2/2) \tag{16}$$

where K is the head loss factor (K-factor) and has the values 0.5 for the entrance, 1.0 for the exit [27]. For duct fittings, elbows, valves, and other heating system losses, a single value of 10 is considered.

The fan efficiency η_{fan} and the motor efficiency η_m are assumed to be 70% and 90%, respectively. Hence, the fan power can be expressed as:

$$P_{fan} = P_{pump}/(\eta_{fan}\eta_m) \tag{17}$$

The thermo-hydraulic efficiency η_{th}, which means the net energy gain divided by the total energy received from the sun, is used to evaluate the thermal performance of the SAC system.

$$\eta_{th} = (P_u - P_{fan})/(IA_p) \tag{18}$$

where P_u means the useful thermal output power which is given by:

$$P_u = (T_{out} - T_{in})c_p\dot{m} \tag{19}$$

3. Experimental verification

Since the theoretical model was deduced and proposed for the first time, its reliability and stability was still uncertain. An indoor experimental system was built to study the performance of a double pass flow SAC under various conditions and verify the accuracy of this mathematical model.

3.1. Experimental setup

In this study, an indoor experimental model system was built in Zhuhai, China, to study the performance of a double pass SAC and compare the measured results with those of the theoretical model.

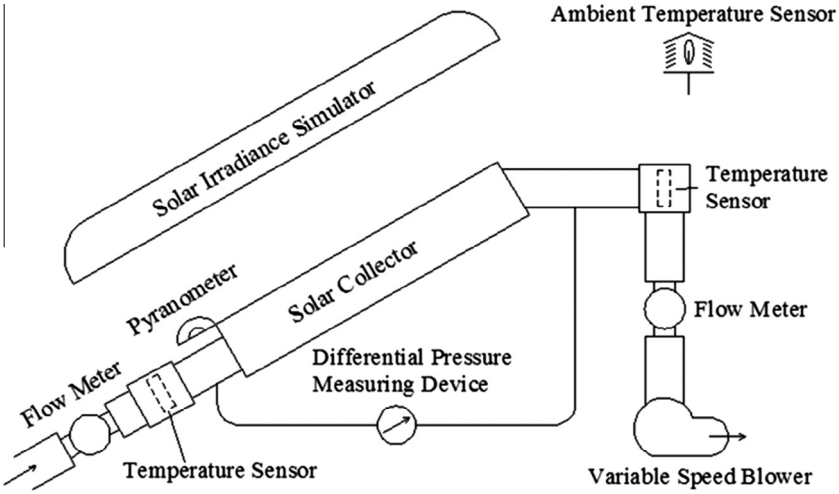

Fig. 3. Schematic diagram of the experimental setup.

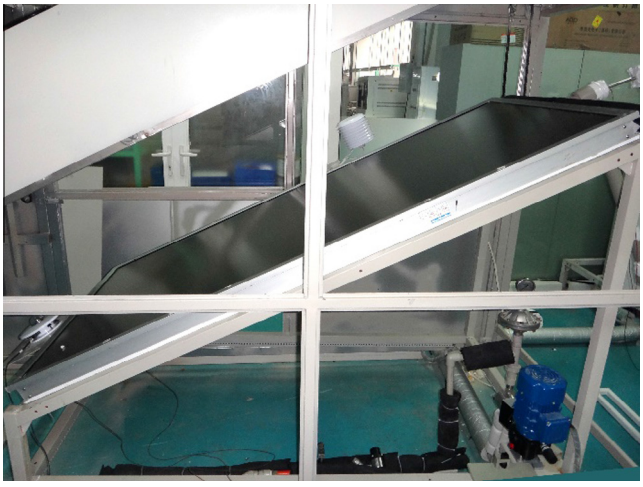

Fig. 4. Photograph of the experimental setup.

A schematic diagram and a photograph of the experimental setup are shown in Figs. 3 and 4.

The experimental setup has been designed, fabricated and tested indoor based on the recommendation of ASHRAE Standard 93-2003 for data collection [28]. The external dimensions of the collector are (length × width × height) 2000 × 1000 × 80 mm. A solar irradiation simulator consisting of eight xenon long-arc lamps was set parallel to the collector plane with a tilt angle of 30°. A variable speed blower was located downstream of the collector to produce a negative gauge pressure in the collector. Omega RTD100 temperature sensors with class A, ±0.15 °C accuracy were used to measure the temperature of the airflow at the upstream, downstream of the SAC as well as the ambient. Turbine flow meters of type LWQ-A produced by Tianjin Sure Instrument Science & Technology Co. Ltd with ±1.5% accuracy were installed at the upstream and downstream of the SAC. The simulated solar irradiance was measured by a pyranometer which was placed parallel to the collector surface. Type TBQ-2A pyranometer produced by Jinzhou Sunshine Technology Co. Ltd with accuracy ±2% was used. The simulated solar irradiance, airflow rate, temperature of the ambient and temperature of the upstream and downstream of the collector were recorded at every 30 s in a data logger (Agilent 34970A). All temperature measurements are carried out by using platinum- resistance thermometers.

Throughout the experiments, airflow rate were varying from 0.02 m^3/s to 0.03 m^3/s, and the simulated solar irradiance were set to constant 800 W/m^2. Prior to each specified experimental period, in which data will be taken, there was a 10 min interval in order to obtain steady-state conditions.

3.2. Experimental study

From these measured data, mass flow rate and collector efficiency were calculated. Equation for mass flow rate is

$$\dot{m} = \dot{V}_{in}\rho_{in} \tag{20}$$

where $\dot{V}_{in}$ and ρ_{in} mean the inlet volume flow rate and the density of the airflow. As the inlet density of flow ρ_{in} is only dependent on the temperature, Eq. (20) can be written as:

$$\dot{m} = f(\dot{V}_{in}, T_{in}) \tag{21}$$

Equation for the solar air collector efficiency is:

$$\eta = \dot{m}c_p(T_{out} - T_{in})/(IA_p) \tag{22}$$

where c_p is the specific heat of air at constant pressure, T_{out} and T_{in} are the outlet and inlet temperature of the airflow, I is the incident solar radiation intensity, A_p is the area of the SAC. If c_p and A_p are considered constant, Eq. (22) can be written as:

$$\eta = f(\dot{m}, T_{out}, T_{in}, I) \tag{23}$$

Then, total uncertainties for mass flow rate and collector efficiency can be written as [29]:

$$\sigma_{\dot{m}} = \left[\left(\frac{\partial \dot{m}}{\partial_{\dot{V}}}\sigma_{\dot{V}}\right)^2 + \left(\frac{\partial \dot{m}}{\partial_{T_{in}}}\sigma_{T_{in}}\right)^2\right]^{1/2} \tag{24}$$

$$\sigma_{\eta} = \left[\left(\frac{\partial \eta}{\partial_{\dot{m}}}\sigma_{\dot{m}}\right)^2 + \left(\frac{\partial \eta}{\partial_{T_{out}}}\sigma_{T_{out}}\right)^2 + \left(\frac{\partial \eta}{\partial_{T_{in}}}\sigma_{T_{in}}\right)^2 + \left(\frac{\partial \eta}{\partial_{I}}\sigma_{I}\right)^2\right]^{1/2} \tag{25}$$

where σ is the uncertainty in the independent variables.

The total uncertainties in determining flow rate and efficiency were estimated by Eqs. (24) and (25). Calculations show that the total uncertainties in calculating mass flow rate of air and efficiency are 2.4% and 3.6%.

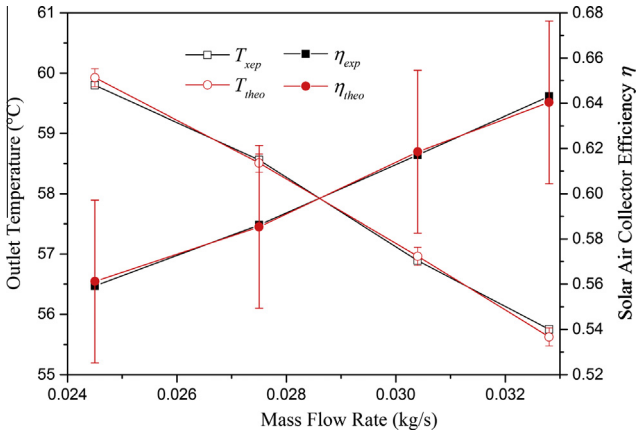

Fig. 5. Comparison of the experimental and theoretical results.

3.3. Comparison of experimental and theoretical results

To test the accuracy of the developed code, the exactly same boundary conditions in the experiments were used in the theoretical study. The computation was repeated for four different conditions that used in the experimental studies. The residual of the outlet temperature was set to be 0.01 °C in the iteration. The comparison of experimental and theoretical results is shown in Fig. 5.

Because of some practical uncertainty in the experimental results, and the assumptions in the theoretical method, the comparison results have some acceptable differences. As shown in Fig. 5, the outlet air temperature results obtained from the theoretical and experimental studies are in reasonable agreement, which supports the validity of the theoretical model used in the studies. The maximum error of temperature increase and thermal efficiency between experimental and theoretical results are 0.36% and 0.41% respectively. Therefore, the mathematical model is available for further analysis and design of SACs.

4. Theoretical results discussion

Having confirmed the accuracy of the mathematical model, it could be used to simulate the performance of a flat plate SAC under various controlled conditions. In order to evaluate the effect of mass flow rate on the thermal performance of the SAC system, a series of values for the environment temperature and solar irradiance are considered. Constant inlet air temperature and ambient wind speed are employed: T_{in} = 21 °C and u_a = 2 m/s. The air specified mass flow rate $\dot{m}$ is varied over the technical range of interest $0.01 \leqslant \dot{m} \leqslant 0.05$ kg/s in steps of 0.005 kg/s. The variation of outlet temperature T_{out} with mass flow rate $\dot{m}$ is shown in Fig. 6.

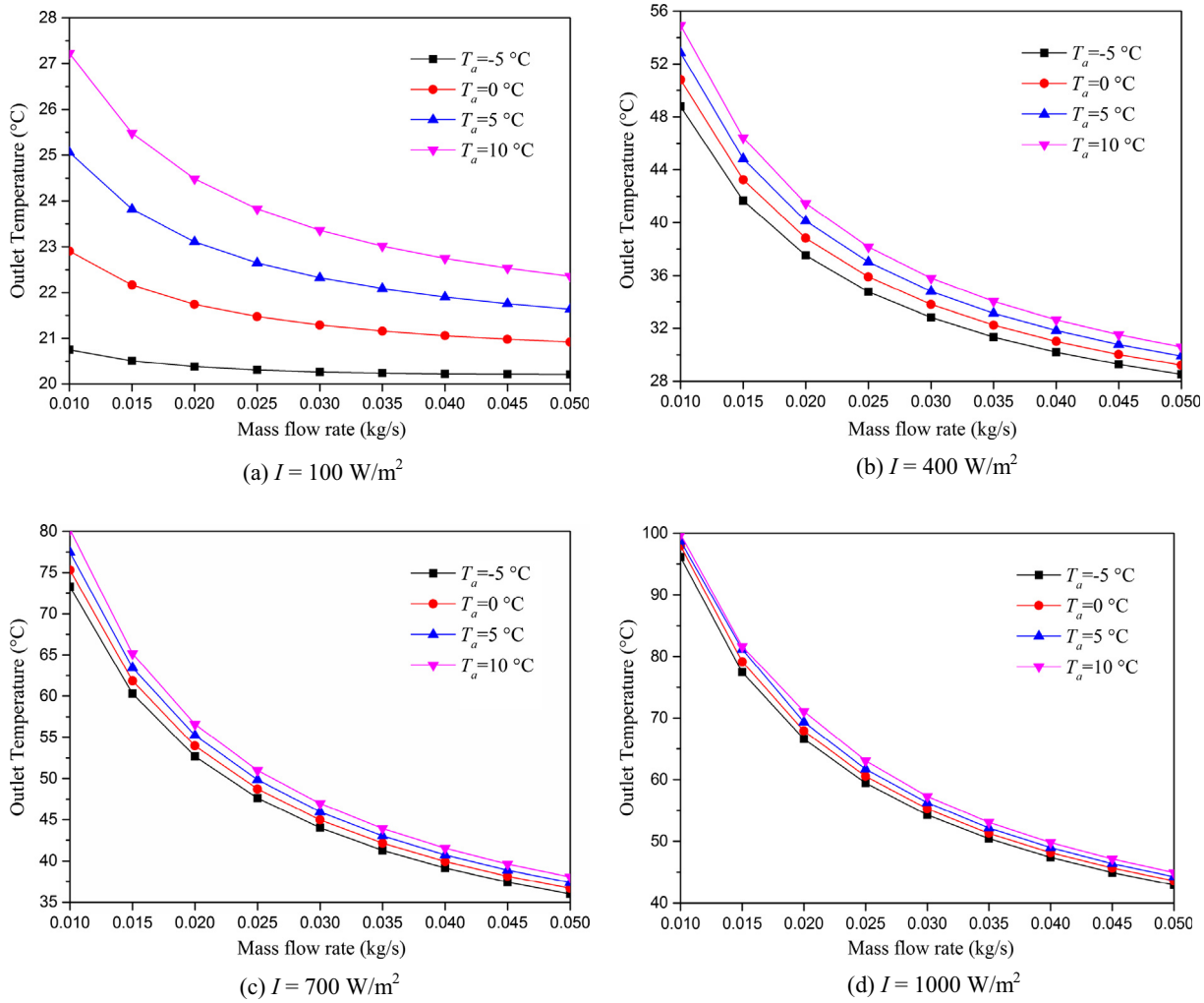

(a) I = 100 W/m^2 (b) I = 400 W/m^2

(c) I = 700 W/m^2 (d) I = 1000 W/m^2

Fig. 6. Variation of outlet temperature T_{out} with mass flow rate $\dot{m}$.

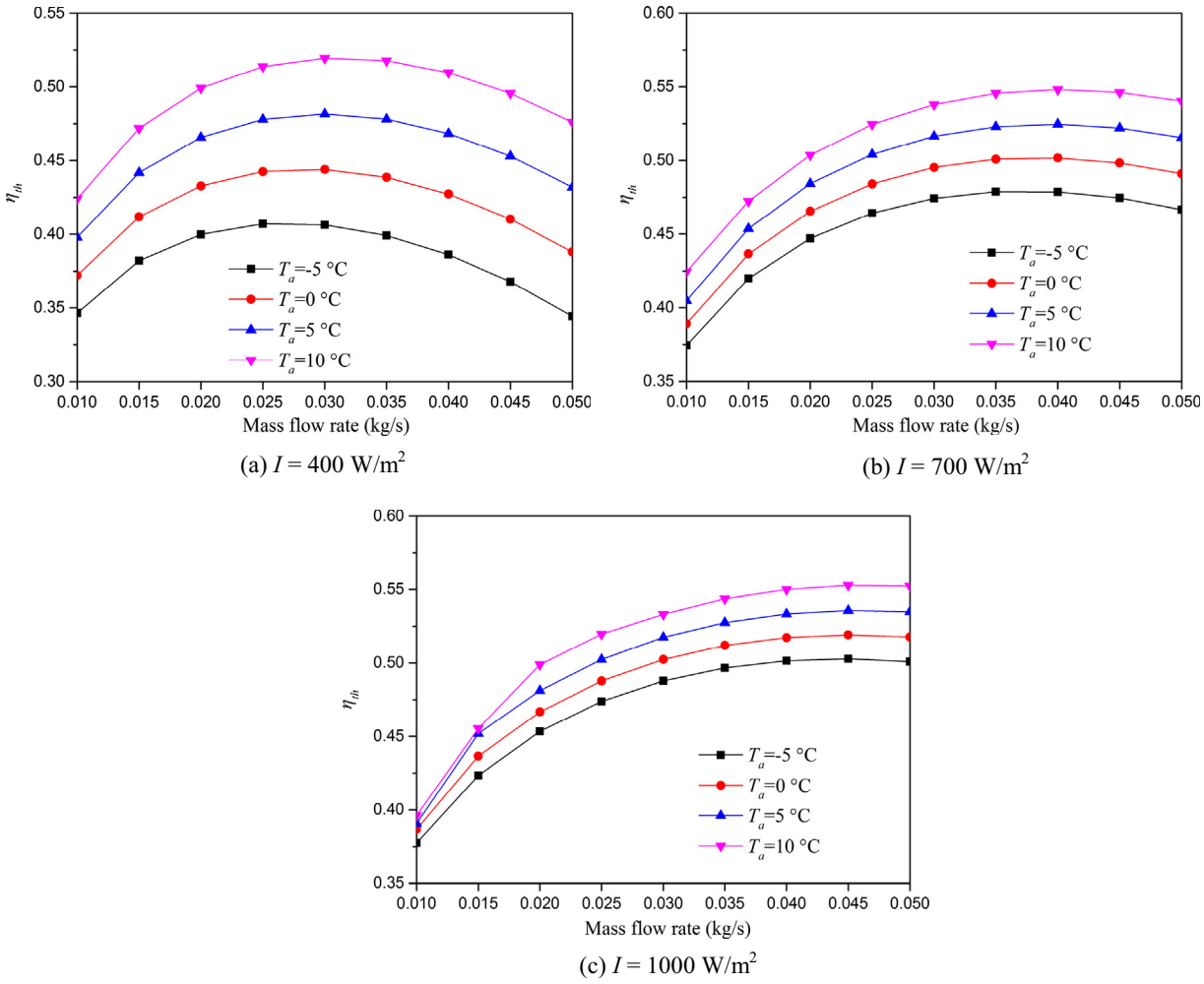

Fig. 7. Variation of thermo-hydraulic efficiency η_{th} with mass flow rate $\dot{m}$.

The results in Fig. 6 show that with the increase of the mass flow rate $\dot{m}$, T_{out} decreases. When $\dot{m}$ gets larger, T_{out} decreases slower. The effect of ambient temperature change on T_{out} is about 0.2 °C/°C, which is very small. As a result, the four lines in each figure have almost the same shape and small difference in the value. For low solar irradiance groups, especially I = 100 W/m^2 as shown in Fig. 6(a), T_{out} is only slightly higher or even lower than T_{in}. Considering the fan power of the SAC, when the air outlet temperature is slightly higher or even lower than the indoor temperature, the SAC experienced losses. Additionally, when the air outlet temperature is low, it is not sufficient to be used as a heat source. Therefore, it is recommended that the SAC be switched off not only during night hours but also when the solar irradiance is lower than 100 W/m^2 in the day, so that it can act as a normally-insulated roof. For this reason, conditions with I = 100 W/m^2 will not be discussed in the thermo-hydraulic performance analyses.

Finally, thermo-hydraulic efficiency values η_{th} for this flat plate SAC are determined for the different rates of airflow employing the procedure described earlier. The variation of η_{th} with $\dot{m}$ is shown in Fig. 7. It is seen that the thermo-hydraulic performance of SAC depends on ambient temperature, solar irradiance and mass flow rate. Under the same solar irradiance, the thermo-hydraulic efficiency increases with the ambient temperature. The influence of the ambient temperature on the thermo-hydraulic efficiency becomes greater when the mass flow rate increases.

Under all environmental conditions, the thermo-hydraulic efficiency increases with the mass flow rate, attains a maximum value at a certain rate $\dot{m}_{opt}$ and, thereafter, decreases with further increase in $\dot{m}$. This is because of the sharp increase in fan power with the increase in airflow rate. When the increase in useful heat gain becomes smaller than the increase in fan power, η_{th} appears to decrease. The $\dot{m}_{opt}$ can be defined as the optimum mass flow rate of the SAC, which depends only on the structure of the SAC and the solar irradiance, and has no apparent relation with the ambient temperature.

For this flat plate SAC, $\dot{m}_{opt}$ equals 0.03 kg/s at I = 400 W/m^2, equals 0.04 kg/s at I = 700 W/m^2, and equals 0.045 kg/s at I = 1000 W/m^2.

5. Conclusions

In the present study, a fast and complete mathematical model based on numerical finite-difference approach under forced convection mode is presented for a flat plate solar air collector. Every part of the SACs, including airflow channel, absorber plate, glass cover, thermal insulation board and fan power is separately modeled. The accuracy of the theoretical model is checked and validated by experiments. From simulations with the mathematical model, the following conclusions have been drawn:

i. The thermo-hydraulic efficiency and outlet air temperature rise along with ambient temperature and solar irradiance.

ii. As the mass flow rate increases, the thermo-hydraulic efficiency increases from the start, attains a maximum value at a certain rate $\dot{m}_{opt}$ and thereafter decreases with further increase of $\dot{m}$.
iii. The increase of mass flow rate $\dot{m}$ has a negative effect on the outlet air temperature, i.e. the outlet air temperature decreases along with the increasing of mass flow rate $\dot{m}$. In addition, with the increase in mass flow rate $\dot{m}$, the influence of ambient temperature on the thermo-hydraulic efficiency increases.
iv. The optimum mass flow rate $\dot{m}_{opt}$ increases along with solar irradiance, $\dot{m}_{opt}$ equals 0.03 kg/s at $I = 400\ W/m^2$, equals 0.04 kg/s at $I = 700\ W/m^2$, and equals 0.045 kg/s at $I = 1000\ W/m^2$. For practical application, the mass flow rate of SAC is suggested to be variable: smaller in the morning and afternoon when the solar irradiance is light and larger at noon when the solar irradiance is strong.

Acknowledgement

The authors are grateful to the National Science & Technology Pillar Program during the "Twelfth Five-Year" Plan Period of China (No. 2014BAJ01B04) for the financial support.

Appendix A

In order to facilitate solving Eqs. (4)–(6), all variables have been transferred into non-dimensionalized form. The methods are as follows:

$$U = u/u_{in} \tag{A1}$$

$$V = v\ Re_{in}Pr_{in}/u_{in} \tag{A2}$$

$$P = (p - p_{in})/\rho_{in}u_{in}^2 \tag{A3}$$

$$X = x/(Re_{in}Pr_{in}W) \tag{A4}$$

$$Y = y/W \tag{A5}$$

$$\Theta = k(T - T_{in})/(WI) \tag{A6}$$

where the subscript "*in*" indicates inlet status parameters. U, V, P, X, Y and Θ represent the non-dimensionalized parameters u, v, p, x, y and T, respectively.

After non-dimensionalization changing, the continuity, momentum and energy equations can be described as:

$$\frac{\partial V}{\partial Y} + \frac{\partial U}{\partial X} = 0 \tag{A7}$$

$$\frac{1}{Pr}\left(U\frac{\partial U}{\partial X} + V\frac{\partial U}{\partial Y}\right) = -\frac{1}{Pr}\frac{dP}{dX} + \frac{\partial^2 U}{\partial Y^2} \tag{A8}$$

$$U\frac{\partial \Theta}{\partial X} + V\frac{\partial \Theta}{\partial Y} = \frac{\partial^2 \Theta}{\partial Y^2} \tag{A9}$$

The following is the non-dimensionalized momentum equation of explicit difference scheme:

$$\frac{1}{Pr}U_{i-1,j}\left(\frac{U_{i,j} - U_{i-1,j}}{\Delta X}\right) + \frac{1}{Pr}V_{i-1,j}\left(\frac{U_{i-1,j+1} - U_{i-1,j-1}}{2\Delta Y}\right) = -\frac{1}{Pr}\frac{(P_i - P_{i-1})}{\Delta X} + \frac{(U_{i-1,j+1} + U_{i-1,j-1} - 2U_{i-1,j})}{\Delta Y^2} \tag{A10}$$

The following is the non-dimensionalized continuity equation of explicit difference scheme:

$$\frac{V_{i,j} - V_{i,j-1}}{\Delta Y} = -\frac{1}{2}\left(\frac{U_{i,j} - U_{i-1,j}}{\Delta X} + \frac{U_{i,j-1} - U_{i-1,j-1}}{\Delta X}\right) \tag{A11}$$

By the means of central difference and transposition, it can be deduced that:

$$\Theta_{i,j} = \left(\Theta_{i-1,j} - A\Delta X\frac{V_{i-0.5,j}}{U_{i-0.5,j}} + B\frac{\Delta X}{U_{i-0.5,j}}\right)\Big/\left(1 + \frac{\Delta X}{U_{i-0.5,j}\Delta Y^2}\right) \tag{A12}$$

where A and B are defined as follows:

$$A = \left(\frac{\Theta_{i-1,j+1} - \Theta_{i-1,j-1} + \Theta_{i,j+1} - \Theta_{i,j-1}}{4\Delta Y}\right) \tag{A13}$$

$$B = \frac{\Theta_{i-1,j+1} + \Theta_{i-1,j-1} - 2\Theta_{i-1,j} + \Theta_{i,j+1} + \Theta_{i,j-1}}{2\Delta Y^2} \tag{A14}$$

Thereafter, the discretization of continuity, momentum and energy equations has been completely fulfilled.

References

[1] Duffie John A, Beckman William A. Solar engineering of thermal processes. 3rd ed. New Jersey: John Wiley & sons; 2006.
[2] Chang Huawei, Duan Chen, Wen Ke, et al. Modeling study on the thermal performance of a modified cavity receiver with glass window and secondary reflector. Energy Convers Manage 2015;106:1362–9.
[3] Close DJ. Solar air heaters for low and moderate temperature applications. Sol Energy 1963;7(3):117–24.
[4] Parker BF et al. Thermal performance of three solar air heaters. Sol Energy 1993;51(6):467–79.
[5] Ong KS. Thermal performance of solar air heaters: mathematical model and solution procedure. Sol Energy 1995;55(2):93–109.
[6] Ong KS. Thermal performance of solar air heaters-experimental correlation. Sol Energy 1995;55(3):209–20.
[7] Njomo D, Daguenet M. Sensitivity analysis of thermal performances of flat plate solar air heaters. Heat Mass Transf 2006;42:1065–81.
[8] Ahmad Fudholi, Kamaruzzaman Sopian, Yusof Othman Mohd, et al. Energy analysis and improvement potential of finned double-pass solar collector. Energy Convers Manage 2013;75:234–40.
[9] Wei Wei, Jie Ji, Tin-Tai Chow, et al. Experimental study of a combined system of solar Kang and solar air collector. Energy Convers Manage 2015;103:752–61.
[10] Camelia Stanciu, Dorin Stanciu. Optimum tilt angle for flat plate collectors all over the World – A declination dependence formula and comparisons of three solar radiation models. Energy Convers Manage 2014;81:133–43.
[11] Maia Cristiana B, Ferreira Andre G, Hanriot Sergio M. Evaluation of a tracking flat-plate solar collector in Brazil. Appl Solar Eng 2014;73:953–62.
[12] Miguel Baritto, Johane Bracamonte. A dimensionless model for the outlet temperature of a nonisothermal flat plate solar collector for air heating. Sol Energy 2012;86:647–53.
[13] Miguel Baritto, Johane Bracamonte. Optimal aspect ratios for non-isothermal flat plate solar collectors for air heating. Sol Energy 2013;97:605–13.
[14] Viorel Badescu. Optimum size and structure for solar energy collection systems. Energy 2006;31:1819–35.
[15] Viorel Badescu. Optimum fin geometry in flat plate solar collector systems. Energy Convers Manage 2006;47:2397–413.
[16] Zamfir E, Badescu V. Different strategies for operation of flat-plate solar collectors. Energy 1994;19:1245–54.
[17] Deniz Alta, Emin Bilgili, Ertekin C, et al. Experimental investigation of three different solar air heaters: energy and exergy analyses. Appl Energy 2010;87:2953–73.
[18] Viorel Badescu. Optimal control of flow in solar collectors for maximum exergy extraction. Int J Heat Mass Transf 2007;50:4311–22.
[19] Farahat S, Sarhaddi F, Ajam H. Exergetic optimization of flat plate solar collectors. Renew Energy 2009;34:1169–74.
[20] Farzad Jafarkazemi, Emad Ahmadifard. Energetic and exergetic evaluation of flat plate solar collectors. Renew Energy 2013;56:55–63.
[21] Bahrehmand D, Ameri M, Gholampour M. Energy and exergy analysis of different solar air collector systems with forced convection. Renew Energy 2015;83:1119–30.
[22] El-Sebaii AA, Aboul-Enein S, Ramadan MRI, et al. Thermal performance investigation of double pass-finned plate solar air heater. Appl Energy 2011;88:1727–39.
[23] Hegazy Adel A. Optimum channel geometry for solar air heaters of conventional design and constant flow operation. Energy Convers Manage 1999;40:757–74.

[24] Hegazy Adel A. Thermohydraulic performance of air heating solar collectors with variable width, flat absorber plates. Energy Convers Manage 2000;41:1361–78.
[25] Tao WQ. Numerical heat transfer. 2nd ed. Xi'an: Xi'an Jiaotong University Press; 2001.
[26] Oosthuizen Patrick H, David Naylor. An introduction to convective heat transfer analysis. Singapore: McGraw-Hill; 1999.
[27] Bernard Massey. Mechanics of fluids. 8th ed. New York: Taylor & Francis; 2006.
[28] ASHRAE Standard 93-2003. Methods of testing to determine the thermal performance of solar collectors, 2003.
[29] Coleman HW, Steele Jr WG. Experimentation and uncertainty analysis for engineers. 2nd ed. New York: Wiley; 1999.